

Adsorption of proteins on nanoporous Ti surfaces

Ludovic Richert^{a,c,1}, Fabio Variola^{a,b,1}, Federico Rosei^b, James D. Wuest^d, Antonio Nanci^{a,*}

^a Laboratory for the Study of Calcified Tissues and Biomaterials, Faculté de Médecine Dentaire, Université de Montréal, Montréal, QC, Canada, H3C 3J7

^b INRS-EMT, Université du Québec, Varennes, QC, Canada, J3X 1S2

^c Faculté de Médecine, Université de Strasbourg, Strasbourg, 67085, France

^d Département de Chimie, Université de Montréal, Montréal, QC, Canada, H3C 3J

ARTICLE INFO

Article history:

Received 1 April 2010

Accepted 5 May 2010

Available online 19 May 2010

Keywords:

Adsorption

Proteins

Titanium

Nanotopography

QCM-D.

ABSTRACT

The cascade of events that regulate cell-substrate interactions is not yet fully understood. However, it is now generally recognized that proteins adsorbed on a substrate prior to its colonization have a major influence on initiating and directing cellular activities. Protein adsorption and the characteristics of the adsorbed layer are determined in part by the physical/chemical properties of the underlying surface. Chemical oxidation can be used to generate nanoscale textures on various metals used as implants in medicine. In this study, we exploit a mixture of H₂SO₄/H₂O₂ to etch sputtered titanium, and we evaluate the adsorption of a broad range of proteins on the resulting nanoporous surface. Untreated and nanoporous surfaces were characterized by scanning electron microscopy (SEM), atomic force microscopy (AFM) and Fourier-transform infrared spectroscopy (FTIR). Protein adsorption was assessed by using a quartz crystal microbalance in conjunction with dissipation monitoring (QCM-D). Our results demonstrate that the network of nanometric pits resulting from controlled chemical oxidation confers to titanium the capacity to differentially regulate protein adsorption. The observed selectivity in adsorption may have a significant impact on initial molecular events that ultimately dictate cell fate and activity.

© 2010 Elsevier B.V. All rights reserved.

1. Introduction

The biocompatibility of implanted materials and the success of prosthetic devices depend on biological events such as cellular adhesion, proliferation, and differentiation, which occur on surfaces in the early stages of tissue integration [1]. Initiation and development of these cellular processes are believed to be affected by an adlayer of proteins adsorbed from bodily fluids onto the implant surface prior to cellular colonization [1–5]. It has been shown that such protein adsorption is sensitive to specific physical/chemical properties of the implant surface under *in vitro* conditions. Wettability [6–9], the charge distribution at the surface [10–12], and morphology [13–15] can all affect the kinetics and thermodynamics of processes involving proteins, including adsorption, orientation, and denaturation [16–18]. It is believed that only topographical features with dimensions similar to those of surface-bound proteins (~10 nm) can significantly affect their morphology and activity [19]. For this reason, recent studies have focused on the influence of nanometric surface features on the adsorption of relevant bioeffector proteins [10,20–23].

In previous work, we demonstrated that simple chemical oxidation with H₂SO₄/H₂O₂ can be exploited to create a nanoporous sponge-like texture on biologically relevant metals such as titanium

[24,25], Ti₆Al₄V [26,27], and CrCoMo [28]. Such nanotopography has been shown to have unique effects on various cellular processes, including the expression of genes and proteins, as well as the differentiation, adhesion, and proliferation of cells [26–31].

In this study, we use this chemical treatment to nanopattern titanium films deposited by sputtering directly on the sensor of a quartz-crystal microbalance (QCM-D), thereby evaluating the influence of oxidative nanopatterning on protein adsorption. The QCM-D technique has been widely used for non-destructive real-time studies of the adhesion of biological entities on different substrates at the liquid–solid interface [32]. Such entities have included proteins [13,20–22], cells [33–35], and bacteria [36,37]. While the majority of the studies in the field focuses on establishing how specific proteins interact with a particular nanostructured surface [10,20–23], in general characterized by nanosized protrusions, our objective was to determine whether the generated nanoporous structure exerts a differential effect on the adsorption of a broad spectrum of proteins. These proteins were selected without any biological bias to reflect differences in molecular weight and isoelectric point. Considering the large number of proteins tested, we have opted to carry out measurements at a single concentration within the range of previously reported studies [16,21,22,38]. In addition, we investigated the effects of the generated nanostructure on platelet adhesion. The results obtained highlight the capacity of nanoporous titanium surfaces obtained by chemical oxidation to differentially modulate protein adsorption *in vitro*.

* Corresponding author.

E-mail address: Antonio.Nanci@umontreal.ca (A. Nanci).

¹ These authors contributed equally.

Table 1

Adsorption time, molecular weight (MW), isoelectric point (pI), and concentration of the proteins used in the study.

Protein	Adsorption time (min)	MW (kDa) ^a	pI ^b	Concentration (μg/mL)	Reported dimension
Bovine serum albumin (BSA) [59]	20	65	4.8–5.1	100	14 × 4 nm
Collagen Type I [60]	20	65	4.5–5.5	100	300 × 1.5 nm
Fibronectin [61]	60	~2 × (220)	5.8–6.3	50	20 nm (diameter)
Fibrinogen [18,62]	60	340	5.1	50	45 × 9 × 6 nm
Rabbit immunoglobulin anti-sheep (IgG) [62]	240	~150	7.4–7.8	100	14.5 × 8.5 × 4 nm
Goat immunoglobulin anti-rabbit Alexa 488 (Anti-IgG)	240	~150		(1:500)	N/A
Human growth/differentiation factor-5 (GDF-5) [49,63]	240	26.8	9.8	100	9.7 × 9.7 × 4.8 nm (crystals)
Lysozyme [58,64,65]	60	14.6	10.5–11.0	100	3 × 3 × 4.5 nm

^a Molecular weights were provided by the supplier.^b Isoelectric points were either calculated by using the algorithm from ExpASY's computer pI/MW program or retrieved from the literature.

2. Materials and methods

2.1. Substrate preparation

Titanium-sputtered gold-coated QCM sensors 14 mm in diameter (QSX 301, Q-Sense, Västra Frölunda, Sweden) were nanopatterned with a 1:1 mixture of 10 N H₂SO₄ (J. T. Baker, Phillipsburg, NJ) and 30% aqueous H₂O₂ (Fisher Scientific, Fair Lawn, NJ), according to a previously established protocol [24]. The titanium-coated sensors were immersed in the oxidizing mixture at room temperature, and etching was arrested after 1 h by adding distilled water. The etched sensors were then washed further with ultra-pure deionized water (18.2 MΩ/cm) in an ultrasonic bath. Prior to QCM measurements with dissipation monitoring (QCM-D) and surface characterization, etched sensors and untreated controls were both rinsed with 100% ethanol and dried in air.

2.2. Protein solutions

Proteins were purchased from Sigma-Aldrich (St. Louis, MO) and were dissolved in D-PBS one day before use. Collagen Type I was first dissolved overnight in 0.1 M acetic acid at 4 °C to produce a concentration of 1 mg/mL. This primary solution was centrifuged at 4500 rpm for 60 min, and the supernatant was removed and brought to a final concentration of 0.1 mg/mL in D-PBS. Detailed information about proteins used and their concentration is summarized in Table 1.

2.3. Platelet preparation

Blood was drawn from the femoral artery of a male Wistar rat (~225 g, Charles River, Wilmington, MA), immediately mixed with citrate solution (3.8 mg/mL of citrate in D-PBS) at 1:10 (v/v) and centrifuged at 160 g (30 min) to eliminate erythrocytes and white blood cells. The supernatant was collected and further centrifuged for 30 min at 3000 g. The resulting platelet-rich plasma plug was re-suspended in citrate solution. Platelets were counted with a hemacytometer and the solution adjusted with the PBS-citrate solution to a concentration of 5 × 10⁶ platelets per mL.

2.4. Surface characterization

Surfaces of etched sensors and untreated controls were examined by using a JEOL-JSM 7400F field-emission scanning electron microscope (SEM, JEOL, Tokyo, Japan) operated at 2 kV. Images were processed by ImageTool (UTHSCSA, Houston, TX) to determine the diameter of the nanopores resulting from chemical oxidation. Atomic force microscopy images of 1 × 1 μm² size were obtained in the tapping mode using a JEOL SPM 5200 microscope. Ultra-sharp silicon tips (SSS-NCHR, Nanosensors, Neuchatel, Switzerland) with a curvature radius of 2 nm were used to minimize the tip-convolution effect. The surface root-mean-square roughness (RMS) was determined

from the images using WSxM software (Nanotec Electrónica S.L., Madrid, Spain).

A Nexus 870 Fourier-transform infrared (FTIR) spectrometer equipped with a SAGA (smart aperture grazing angle) accessory (Thermo Nicolet, Madison, WI) was used to probe the native and modified titanium oxide layer resulting from chemical oxidation. Analysis of the thin oxide layer was performed in grazing angle mode at an angle of 80° with respect to the surface normal, using a spectral resolution of 4 cm⁻¹ in the 475–4000 cm⁻¹ range. Spectroscopic information was collected from an 8 mm diameter area. A gold substrate was used to collect a background spectrum. Spectra were finally fitted by PeakFit software (SPSS, Chicago, IL) as reported

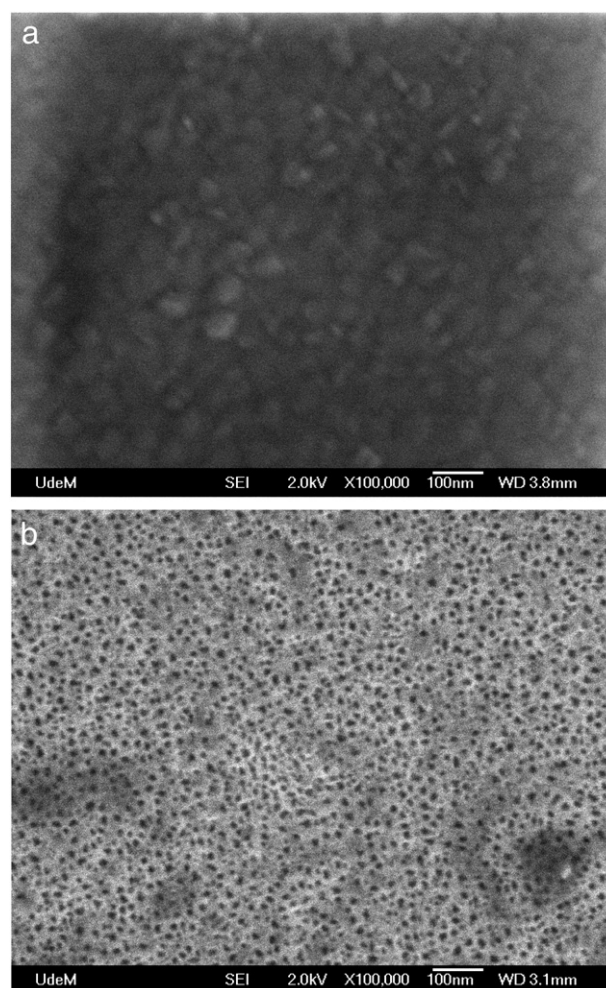


Fig. 1. SEM images of sputtered titanium before (a) and after (b) treatment with H₂SO₄/H₂O₂.

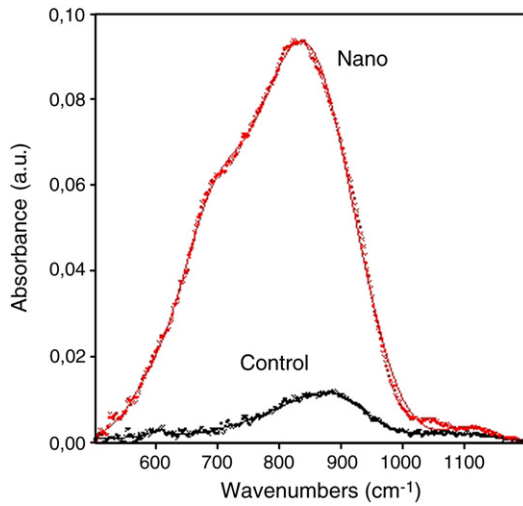


Fig. 2. FTIR spectra of sputtered titanium before (Control) and after (Nano) treatment with $\text{H}_2\text{SO}_4/\text{H}_2\text{O}_2$.

previously [25]. The integral area of the absorption band in the $475\text{--}1100\text{ cm}^{-1}$ range was used to estimate the oxide thickness [27,28,39].

2.5. QCM-D

Prior to each measurement, the QCM-D chamber (Q-Sense AB, Gothenburg, Sweden) was rinsed thoroughly with ultra-pure deionized water equilibrated with D-PBS to obtain a stable Δf and ΔD baseline signal. After QCM-D readings in D-PBS reached a stable value, protein solutions were injected. Frequency (Δf) and dissipation (ΔD) shifts were measured in real-time during protein injection and for variable periods required by each protein to reach adsorption equilibrium (Table 1). Simultaneous measurements of Δf and ΔD data were acquired for the 3rd overtone (15 MHz). After each measurement, the chamber was washed twice with D-PBS and then rinsed with 10 mM sodium dodecyl sulfate (SDS) for 30 min. Similarly, sensors were sonicated for 30 min in 10 mM SDS, placed in an UV-ozone oven for 10 min, and successively rinsed twice with ultra-pure deionized water before reuse. All experiments were performed at 37°C and replicated three times. For data acquisition and data analysis, the software packages QSoft and QTools, respectively, were used.

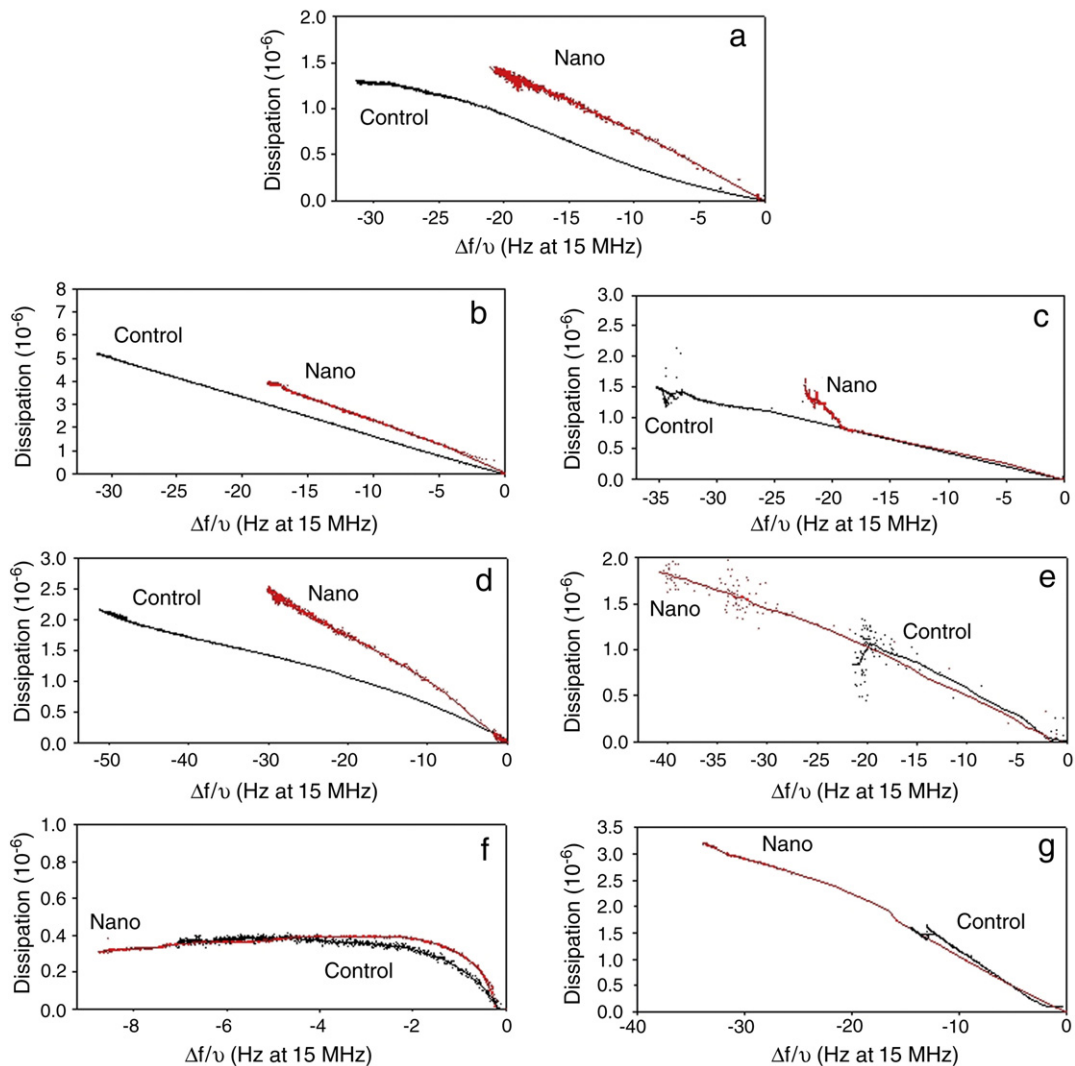


Fig. 3. Representative plots of ΔD as a function of Δf for the 3rd overtone (15 MHz) of a) IgG (100 mg/mL); b) collagen I (100 mg/mL); c) BSA (100 mg/mL); d) fibronectin (50 mg/mL); e) fibrinogen (50 mg/mL); f) GDF-5 (100 mg/mL); and g) lysozyme (100 mg/mL), on sputtered (Control) and nanoporous (Nano) titanium.

3. Results

Figure 1a and b displays SEM micrographs of titanium surfaces grown by sputtering, before and after chemical treatment. Untreated substrates exhibited no distinctive topographical patterns. The coating process produced surfaces with a grainy appearance similar to those produced by e-gun evaporation of tantalum (Fig. 1a) [20,21,40]. In contrast, oxidized surfaces showed an array of nanopores across the surface (Fig. 1b). Detailed image analysis determined that the main pit diameter was 12 ± 5 nm.

Quantitative changes in the surface root-mean-square roughness (RMS) assessed by AFM analysis confirmed that a significant topographical alteration is produced by chemical treatment. Before etching, titanium-coated substrates showed a roughness value of 1.7 ± 0.2 nm, which increased to 2.5 ± 0.4 nm after etching.

Figure 2 displays shows IR absorption in the $475\text{--}1100\text{ cm}^{-1}$ range for etched substrates and untreated controls. The two bands located at approximately at 600 and 800 cm^{-1} were assigned to Ti–O stretching vibrations [41,42]. The total area of the Ti–O absorption peak was demonstrated to be proportional to the thickness of the oxide layer [27,43]. The ratio of the thicknesses of the oxide layers of untreated and treated substrates can be thus approximated by the ratio of integral areas, which was estimated to be about 10. Because the thickness of the native oxide layer on titanium is about 5 nm [25,44], we can estimate a thickness of about 50 nm on nanopatterned substrates.

In the QCM technique, the adsorption of a thin layer of mass on the surface of a quartz sensor induces a decrease in its resonant frequency (f). For a rigid layer, the frequency shift is correlated with the adsorbed mass according to the Sauerbrey relation: $\Delta m = -C\Delta f/\nu$, where ν is the overtone number (1, 3, 5, 7) [45] and C is equal to $17.7\text{ ng/cm}^2\text{ Hz}$ for the AT-cut crystal used in the experiment.

Frequency and dissipation shifts for the proteins used in this study exhibited only a small (<10%) overtone dependence and a relatively low dissipation ($\Delta D_n \sim 8\text{--}10 \times 10^{-6}$) [46]. In such cases, the experimental results can be approximated by the Sauerbrey relation [18,46]. Differences in adsorbed mass were estimated in terms of percentage difference referred to controls, $\left(\frac{\Delta f_{\text{Nano}} - \Delta f_{\text{Control}}}{\Delta f_{\text{Control}}} * 100\right)$, between frequency shifts measured on control ($\Delta f_{\text{Control}}$) and etched (Δf_{Nano}) substrates. The slope of the $\Delta D/\Delta f$ plots was used to compare the viscoelastic properties (i.e. dissipation of the layer, directly related to its rigidity) of adlayers adsorbed on control and etched substrates.

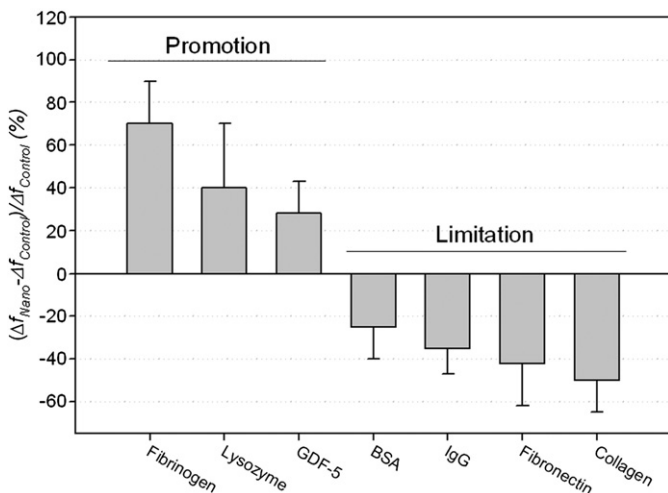


Fig. 4. Influence of nanotopography on the adsorption of proteins. The results illustrated derive from three measurements and are expressed in terms of percentage difference between frequency shifts on unmodified and nanopatterned titanium surfaces compared to untreated substrates (controls). Error bars indicate the standard deviation over three sets of measurements.

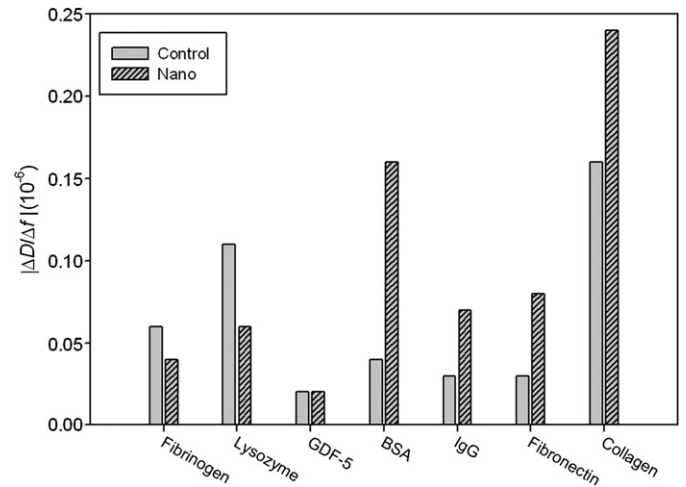


Fig. 5. $|\Delta D/\Delta f|$ values of the measurements illustrated in Fig. 3 for proteins adsorbed on untreated (Control) and nanopatterned (Nano) surfaces.

Figure 3a–g displays the $\Delta D/\Delta f$ plots of the seven different proteins dissolved in phosphate buffer (pH 7.4). The frequency shift values were normalized by $n=3$ according to the Sauerbrey equation [45]. Clearly, the QCM response varies significantly according to the substrate, as measured by the total mass adsorbed and the viscoelasticity of the adsorbed layer. In fact, all $\Delta D/\Delta f$ plots presented in Fig. 3 show adsorption curves for control and nanopatterned surfaces that differ in the final frequency shift (proportional to the mass uptake) and/or in the slope (proportional to the viscoelasticity of the adsorbed layer). To better present these variations in protein adsorption on the two different substrates, we plotted the percentage differences of frequency shifts (Fig. 4). At the chosen concentration, adsorption of proteins such as fibrinogen and lysozyme was considerably promoted on nanopatterned surfaces, for an average total mass uptake increase of 70 and 40%, respectively, compared with untreated controls. Similarly, the adsorption of GDF-5 was affected by the nanoporous surface, but to a lesser extent (30%). On the other hand, the adsorption of collagen, fibronectin, IgG, and BSA was significantly limited (minus 20–50%) on treated substrates.

The $\Delta D/\Delta f$ ratios presented in Fig. 5 illustrate the viscoelastic properties of the adsorbed protein layers. For some proteins (fibrinogen and GDF-5), the $\Delta D/\Delta f$ ratio presents similar values on treated and untreated surfaces, thus indicating similar viscoelastic properties of the adsorbed layers. However, others (lysozyme, IgG, BSA, fibronectin, and collagen) show significantly different behaviors. We also monitored the adsorption of anti-IgG on the IgG adlayer (Fig. 6). As observed for IgG, the adsorbed mass of anti-IgG is about 35% less on nanoporous surfaces compared with the control.

In the case of platelets, Fig. 7a demonstrates that frequency shifts (i.e. $\Delta f/\nu$) measured by the QCM-D technique are higher (about 25%) on nanoporous surfaces. The Sauerbrey equation cannot be applied to this case due to the high variations of Δf at different overtones and to

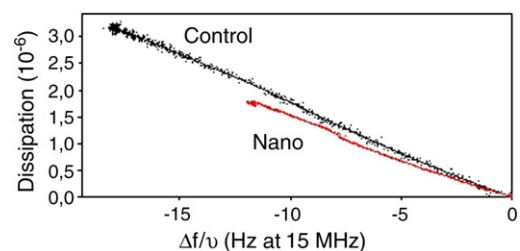


Fig. 6. $\Delta D/\Delta f$ plot (at 15 MHz) of anti-IgG adsorbed on control and nanoporous titanium surfaces after initial adsorption of IgG.

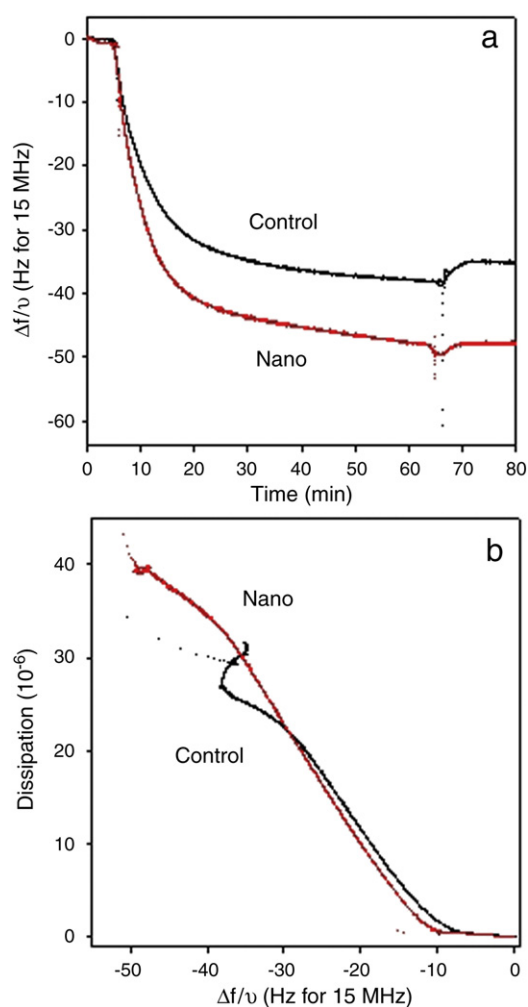


Fig. 7. a) Evolution of $\Delta f/v$ (at 15 MHz) during adsorption of platelets on control and nanoporous surfaces. b) $\Delta D/\Delta f$ plot for platelets on untreated (Control) and nanoporous (Nano) titanium surfaces.

high dissipations (Fig. 7b); however we can infer that the adsorption of platelets is enhanced on nanoporous surfaces.

4. Discussion

Our observations show that chemical oxidation with H_2SO_4/H_2O_2 , which was developed for bulk implantable metals, also efficiently creates nanoscale patterns on thin layers of sputtered titanium. However, analysis of SEM images demonstrated that the resulting nanoporosity differs from that observed with bulk metals. The surface of oxidatively treated sputtered titanium showed an array of well-defined nanosized pits, whereas those of similarly treated cpTi, Ti6Al4V, tantalum, and CrCoMo are characterized by a nanoscale network [28]. The mean diameter of the pores on sputtered titanium (~ 11 nm) was found to be significantly smaller than what has been previously found (~ 20 nm) for nanopores constituting the sponge-like network on bulk titanium (cpTi) [25]. The nanosized pits that form on sputtered titanium are similar to the ones created on poly (methyl methacrylate) (PMMA) by electron-beam lithography (EBL) and used to evaluate the effects of nanometric cues on the differentiation of stem cells [47].

Although oxidative patterning on bulk and sputtered titanium gives rise to different topographical features and surface roughnesses, the process leads to similar increases in the thickness of the surface oxide layer, suggesting that the extent of oxidation is independent of the initial surface features. Oxidative treatment yielded a significant

increase in the surface RMS roughness of the sputtered titanium layers (2.5 ± 0.4 nm vs. 1.7 ± 0.2 nm). It is well known that roughness affects the frequency and dissipation responses of the QCM technique [40,48]. Effects of surface topography on Δf and/or ΔD can thus be misinterpreted as variations in the adsorbed mass and/or in the viscoelastic properties of the adlayer. However, it was demonstrated that surface roughnesses below ~ 3 nm do not affect frequency and dissipation responses, and that only those larger than ~ 6 nm cause significant frequency shifts [40]. Because RMS measurements for both control and treated surfaces were all below 3 nm, and because these measurements are not likely to be significantly affected by tip-deconvolution effects (minimized by the use of ultra-sharp AFM tips), we conclude that the observed frequency and dissipation shifts must therefore be mainly derived from protein adsorption.

Even though our results do not quantitatively address the kinetics and thermodynamics of adsorption of the proteins we tested, they nonetheless allow us to conclude that nanoporosity created by chemical oxidation gives sputtered titanium the capacity to enhance or limit protein adsorption selectively. At the tested concentration, adsorption of proteins such as lysozyme, fibrinogen, and GDF-5 was promoted, whereas the adsorption of collagen, fibronectin, BSA, and IgG was significantly reduced. The ability to enhance the adsorption of GDF-5 is particularly noteworthy because this growth factor stimulates the adhesion and differentiation of osteogenic cells [49–51].

The size of proteins may in part explain this behavior. In fact, the two proteins that have overall dimensions that can be accommodated within the nanopits, GDF-5 and lysozyme, exhibit enhanced adsorption, suggesting that 1) the surface array of pits may function at least in part as a physical entrapment and/or 2) the greater surface area resulting from the creation of the nanoporous structure provides more binding sites. In addition, in the case of fibronectin and fibrinogen, although these two proteins are characterized by similar molecular weights and isoelectric points, the size of fibronectin (round shape, 20 nm in diameter) may have prevented it from integrating within the pores (approximately 11 nm in diameter), whereas the geometry of fibrinogen (elongated shape) could permit accommodation within the nanotexture. If so, it would be expected that the more complex sponge-like network created on bulk titanium, whose nanopores are larger in diameter, would be more efficient in adsorbing molecules. This property could therefore be exploited to improve the adsorption of small bioactive peptides on the surface of implantable biomaterials. However, it is important to note that the behavior of proteins may vary when they are components in complex mixtures, where competitive adsorption and protein displacement together determine the final adsorption profile [52].

The quantity $|\Delta D/\Delta f|$ expresses the dissipation shift per frequency unit and estimates a characteristic relaxation time of the adlayers [21]. Changes in dissipation are attributed to conformational changes in the structure of the protein layer and/or to the amount of water bound in the layer [18]. The higher the $|\Delta D/\Delta f|$ slope, the higher the dissipation per unit added mass, signaling a less rigid protein layer [53]. Also, the higher the $|\Delta D/\Delta f|$ slope, the lower the affinity of a particular protein for the substrate, resulting in a layer that is more weakly attached to the surface and contains more water [18,53]. $\Delta D/\Delta f$ plots should be interpreted with caution, because $\Delta D/\Delta f$ varies with concentration [18]. However, based on these considerations, we can conclude that the nanotexture generated by oxidative nanopatterning with H_2SO_4/H_2O_2 creates nanometric physical/chemical cues that can affect the final viscoelastic characteristics of the protein adlayers. In particular, our results suggest that proteins whose adsorption is limited by the nanotextured surface (i.e. BSA, IgG, fibronectin, and collagen) create a more dissipative adlayer (the $|\Delta D/\Delta f|$ slope for these proteins is higher on treated surfaces than on controls). This implies that the nanometric pattern affects intermolecular cohesion. It cannot be ruled out that some of the changes in these properties may in part be due to protein denaturation. However, the percentage difference between

the mass adsorbed on control and nanopatterned surfaces remains constant following exposure to anti-IgG. This indicates that presentation and availability of the antigenic sites is not affected by nanoporosity, thereby suggesting minimal denaturation, at least for immunoglobulin.

Several earlier studies have assessed how micron- or submicron-scale modifications of surfaces affect the adsorption of proteins. Surfaces that have been machined, acid-etched, and blasted [15,54,55], as well as submicrometric porous titanium surfaces [14], all show increased adsorption of plasma proteins such as albumin, IgG, fibronectin, and fibrinogen. Although such surface modifications are apparently effective, the origin of the phenomenon is unclear because the modifications are too coarse in lateral size to influence the adsorption of proteins directly. As a consequence, surfaces with nanoscale roughness have been generated on titanium [56], tantalum [20,21], and platinum [22], with the aim of creating surface cues with dimensions similar to those of proteins. These studies have indicated that the adsorption of fibrinogen, albumin, and fibronectin is generally enhanced by nanoroughness, although the effect is not always significant [56]. In agreement with these previous results, our data confirm that the adsorption of fibrinogen is promoted and that the fibronectin adlayer is more rigid on surfaces with nanoscale features. Conversely, our results differ from those reported for the adsorption of albumin, IgG, and fibronectin. The differences may arise from the fact that our surfaces present a network of nanometric pits, whereas other surfaces exhibit nanoscale protrusions. In addition, other experimental parameters known to affect adsorption, including adsorption time [13] and protein concentration [14], are different in other studies. The ability to promote the adsorption of GDF-5, while limiting that of fibronectin, is expected to result in the differential capacity of nanopatterned surfaces to selectively dictate cell behavior, since these two proteins are believed to stimulate the adhesion of bone cells and fibroblasts respectively [49,50,57]. This may partially explain why Ti6Al4V treated with H₂SO₄/H₂O₂ under our conditions has a uniquely selective ability to promote adhesion and proliferation in the case of osteoblasts, but to hamper in the case of fibroblasts [26,27].

The enhanced adsorption of fibrinogen on nanopatterned surfaces would be expected to affect the adsorption of platelets, since fibrinogen plays an important role in the blood coagulation cascade [18]. In fact, this is what we observed, but further studies are needed to determine whether the enhanced adhesion of platelets results from the promoted adsorption of any fibrinogen present in the platelet-rich plasma or from a direct effect of the surface. Platelets are believed to stimulate bone repair and formation [58], so any increase in their adsorption will likely stimulate osteogenic events. Therefore, nanopatterning titanium-coated implants can become a valuable strategy to improve the osseo-integration of biomedical devices. In addition, deposition of thin films of titanium on materials that are not readily amenable to chemical oxidation can be advantageously exploited to create nanotextures on them.

5. Conclusions

In this paper, we have demonstrated for the first time that a simple chemical approach can be efficiently exploited to create an array of nanopores on thin titanium films deposited on a QCM-D sensor. This approach can be further exploited for detailed studies of the effects of nanoporosity on the *in vitro* adsorption of biological molecules.

Our results add additional support to the concept that nanoscale surface cues are pivotal in controlling and guiding biological and molecular events. Using a variety of biologically-relevant proteins, we have shown that their adhesion, as well as their viscoelastic properties, strongly depend on the physical/chemical features of surfaces. In particular, we have reported clear evidence that surfaces exert a differential activity on proteins by promoting or limiting their adhesion to the substrate.

To understand in detail the dynamics of adsorption of each protein tested, further studies will be needed. Caution must be exercised in extrapolating results from *in vitro* analyses to the complex biological environment of the body, but our results reaffirm that QCM sensors with selectively nanostructured surfaces are a powerful tool that can be used to more fully explain biological responses to nanostructured materials.

Acknowledgments

F.V. acknowledges the Canadian Bureau for International Education (CBIE) and FQRNT (Fonds Québécois de la Recherche sur la Nature et les Technologies) for financial support. This work was supported by NSERC (Natural Sciences and Engineering Research Council of Canada) and CIHR (Canadian Institutes of Health Research). J. D. W. and F. R. acknowledge additional support from FQRNT and the CRC (Canada Research Chairs) program. A. N. and F. R. are grateful to NSERC for support through a CRD (Collaborative Research and Development) program with Plasmionique, Inc. Infrastructure support from the CFI (Canadian Foundation for Innovation) is also acknowledged.

References

- [1] K. Anselme, *Biomaterials* 21 (2000) 667.
- [2] B. Kasemo, *Surf. Sci.* 500 (2002) 656.
- [3] D.A. Puleo, A. Nanci, *Biomaterials* 20 (1999) 2311.
- [4] C.J. Wilson, R.E. Clegg, D.I. Leavesley, M.J. Pearcy, *Tissue Eng.* 11 (2005) 1.
- [5] P. Roach, D. Eglin, K. Rohde, C.C. Perry, *J. Mater. Sci. Mater. Med.* 18 (2007) 1263.
- [6] P. Cha, A. Krishnan, V.F. Fiore, E.A. Vogler, *Langmuir* 24 (2008) 2553.
- [7] Y. Arima, H. Iwata, *Biomaterials* 28 (2007) 3074.
- [8] R. Tzoneva, N. Fauchoux, T. Groth, *Biochim. Biophys. Acta* 1770 (2007) 1538.
- [9] L.-C. Xu, C.A. Siedlecki, *Biomaterials* 28 (2007) 3273.
- [10] E.M. Blanco, M.A. Horton, P. Mesquida, *Langmuir* 24 (2008) 2284.
- [11] M. Skepo, *J. Chem. Phys.* 129 (2008) 185101.
- [12] T. Hagiwara, T. Sakiyama, H. Watanabe, *Langmuir* 25 (2009) 226.
- [13] S.R. Sousa, M.M. Bras, P. Moradas-Ferreira, M.A. Barbosa, *Langmuir* 23 (2007) 7046.
- [14] E. Jansson, P. Tengvall, *Colloids Surf. B35* (2004) 45.
- [15] M.N. Sela, L. Badrhi, G. Rosen, D. Steinberg, D. Kohavi, *Clin. Oral Implants Res.* 18 (2007) 630.
- [16] P. Roach, D. Farrar, C.C. Perry, *J. Am. Chem. Soc.* 127 (2005) 8168.
- [17] P. Roach, D. Farrar, C.C. Perry, *J. Am. Chem. Soc.* 128 (2006) 3939.
- [18] A.G. Hemmersam, M. Foss, J. Chevallier, F. Besenbacher, *Colloids Surf. B43* (2005) 208.
- [19] B. Kasemo, *J. Gold, Adv. Dent. Res.* 13 (1999) 8.
- [20] K. Rechendorff, M.B. Hovgaard, M. Foss, V.P. Zhdanov, F. Besenbacher, *Langmuir* 22 (2006) 10885.
- [21] M.B. Hovgaard, K. Rechendorff, J. Chevallier, M. Foss, F. Besenbacher, *J. Phys. Chem. B112* (2008) 8241.
- [22] A. Dolatshahi-Pirouz, K. Rechendorff, M.B. Hovgaard, M. Foss, J. Chevallier, F. Besenbacher, *Colloids Surf. B66* (2008) 53.
- [23] F.A. Denis, P. Hanarp, D.S. Sutherland, J. Gold, C. Mustin, P.G. Rouxhet, Y.F. Dufrene, *Langmuir* 18 (2002) 819.
- [24] A. Nanci, J.D. Wuest, L. Peru, P. Brunet, V. Sharma, S.F. Zalzal, M.D. McKee, *J. Biomed. Mat. Res.* 40 (1998) 324.
- [25] J.-H. Yi, C. Bernard, F. Variola, S.F. Zalzal, J.D. Wuest, F. Rosei, A. Nanci, *Surf. Sci.* 600 (2006) 4613.
- [26] L. Richert, F. Vetrone, J.-H. Yi, S.F. Zalzal, J.D. Wuest, F. Rosei, A. Nanci, *Adv. Mat.* 20 (2008) 1488.
- [27] F. Variola, J.-H. Yi, L. Richert, J.D. Wuest, F. Rosei, A. Nanci, *Biomaterials* 29 (2008) 1285.
- [28] F. Vetrone, et al., *Nanoletters* 9 (2009) 659.
- [29] P.T.d. Oliveira, S.F. Zalzal, K. Irie, A. Nanci, *J. Histochem. Cytochem* 51 (2003) 633.
- [30] P.T.d. Oliveira, A. Nanci, *Biomaterials* 25 (2004) 403.
- [31] P.T.d. Oliveira, S.F. Zalzal, M.M. Beloti, A.L. Rosa, A. Nanci, *J. Biomed. Mat. Res A80* (2007) 554.
- [32] M.A. Cooper, V.T. Singleton, *J. Mol. Recognit.* 20 (2007) 154.
- [33] J. Redepenning, T.K. Schlesinger, E.J. Mechalke, D.A. Puleo, R. Bizioss, *Anal. Chem.* 65 (1993) 3378.
- [34] K.A. Marx, T. Zhou, M. Warren, S.J. Braunhut, *Biotechnol. Prog.* 19 (2003) 987.
- [35] D.M. Gryte, M.D. Ward, W.S. Hu, *Biotechnol. Prog.* 9 (1993) 105.
- [36] A.L. Schofield, T.R. Rudd, D.S. Martin, D.G. Fernig, C. Edwards, *Biosens. Bioelectron.* 23 (2007) 407.
- [37] H.C. Han, Y.R. Chang, W.L. Hsu, C.Y. Chen, *Biosens. Bioelectron.* 24 (2009) 1543.
- [38] A.A. Vertegel, R.W. Siegel, J.S. Dordick, *Langmuir* 20 (2004) 6800.
- [39] F. Variola, A. Nanci, F. Rosei, *Appl. Spectrosc.* 63 (2009) 1187.
- [40] K. Rechendorff, M.B. Hovgaard, M. Foss, F. Besenbacher, *J. Appl. Phys.* 101 (2007) 114502.

- [41] D. Velten, V. Biehl, F. Aubertin, B. Valeske, W. Possart, J. Breme, J. Biomed. Mat. Res. 59 (2002) 18.
- [42] R. Urlaub, U. Posset, R. Thull, J. Non Cryst Solids 265 (2000) 276.
- [43] B. Trasferetti, C. Davanzo, R. Zoppi, N. Cruz, M. Moraes, Phys Rev B. 64 (2001) 125404.
- [44] C. Sittig, M. Textor, N.D. Spencer, M. Wieland, P.-H. Vallotton, J. Mater. Sci. Mater. Med. 10 (1999) 35.
- [45] C. Modin, A.-L. Stranne, M. Foss, M. Duch, J. Justesen, J. Chevallier, L.K. Andersen, A.G. Hemmersam, F.S. Pedersen, F. Besenbacher, Biomaterials 27 (2006) 1346.
- [46] M.B. Hovgaard, M. Dong, D.E. Otzen, F. Besenbacher, Biophys. J. 93 (2007) 2162.
- [47] M.J. Dalby, N. Gadegaard, R. Tare, A. Andar, M.O. Riehle, P. Herzyk, C.D.W. Wilkison, R.O.C. Oreffo, Nat. Mater. 6 (2008) 997.
- [48] M. Urbakh, L. Daikhin, Phys. Rev. B49 (1994) 4866.
- [49] P. Buxton, C. Edwards, C.W. Archer, P. Francis-West, J. Bone Joint Surg. 83A (2001) 23.
- [50] Q. Zeng, X. Li, G. Beck, G. Balian, F.H. Shen, Bone 40 (2007) 374.
- [51] P.T.d. Oliveira, M.A.d. Oliva, W.M.A. Maximiano, K.E.V. Sebastiao, G.E. Crippa, Pietro Ciancaglini, M.M. Beloti, A. Nanci, A.L. Rosa, J. Histochem. Cytochem. 56 (2008) 629.
- [52] H. Noh, E.A. Vogler, Biomaterials 28 (2007) 405.
- [53] F. Hook, M. Rodahl, P. Brzezinski, B. Kasemo, Langmuir 14 (1998) 729.
- [54] R. Silvennoinen, V. Vetterl, S. Hason, H. Tuononen, M. Silvennoinen, K. Myller, L. Cvrcek, J. Vanek, P. Prachar, Opt. Express 16 (2008) 10130.
- [55] F. Luthen, R. Lange, P. Becker, J. Rychly, U. Beck, J.G.B. Nebe, Biomaterials 26 (2005) 2423.
- [56] K. Cai, J. Bossert, K.D. Jandt, Colloids Surf. B49 (2006) 136.
- [57] K.S. Midwood, Y. Mao, H.C. Hsia, L.V. Valenick, J.E. Schwarzbauer, J. Investig. Dermatol. Symp. Proc. 11 (2006) 73.
- [58] H.F. Langer, M. Gawaz, Basic Res. Cardiol. 103 (2008) 299.
- [59] G. Yampolskaya, D. Platikanov, Adv. Colloid Interface Sci. 128–130 (2006) 159.
- [60] Q. Chen, S. Xu, R. Li, X. Liang, H. Liu, J. Colloid Interface Sci. 316 (2007) 1.
- [61] J.R. Hull, G.S. Tamura, D.G. Castner, Biophys. J. 93 (2007) 2852.
- [62] B. Lassen, M. Malmsten, J. Colloid Interface Sci. 180 (1996) 339.
- [63] T.D. Mueller, M. Gottermeier, W. Sebald, J. Nickel, Acta Cryst. F61 (2005) 134.
- [64] A. Bentaleb, V. Ball, Y. Haikel, J.C. Voegel, P. Schaaf, Langmuir 13 (1997) 729.
- [65] T.J. Su, J.R. Lu, R.K. Thomas, Z.F. Cui, J. Penfold, J. Colloid Interface Sci. 203 (1998) 419.